Absorption efficiency and physical bounds on antennas

Gustafsson, Mats; Cismasu, Marius; Nordebo, Sven

2010

CODEN:LUTEDX/(TEAT-7200)/1-20/(2010)

Absorption Efficiency and Physical Bounds on Antennas

Mats Gustafsson, Marius Cismasu, and Sven Nordebo

Electromagnetic Theory
Department of Electrical and Information Technology
Lund University
Sweden

Mats Gustafsson, Marius Cismasu
{Mats.Gustafsson,Marius.Cismasu}@eit.lth.se

Department of Electrical and Information Technology
Electromagnetic Theory
Lund University
P.O. Box 118
SE-221 00 Lund
Sweden

Sven Nordebo
sven.nordebo@lnu.se

School of Computer Science
Physics and Mathematics
Linnaeus University
SE-351 95 Växjö
Sweden

Department of Electrical and Information Technology
Electromagnetic Theory
Lund University
P.O. Box 118
SE-221 00 Lund
Sweden

Editor: Gerhard Kristensson

Abstract

The all spectrum absorption efficiency appears in the physical bounds on antennas expressed in the polarizability dyadics. Here, it is shown that this generalized absorption efficiency is close to 1/2 for small idealized dipole antennas and for antennas with a dominant resonance in their absorption. Also, the usefulness of this parameter is analyzed for estimation of antenna performance. The results are illustrated with numerical data for several antennas.

1 Introduction

A new set of physical bounds on antennas was introduced in [4–7, 16]. These bounds relate the performance of the antenna to the electro- and magneto-static polarizability dyadics of a circumscribing geometry. This generalizes the classical bounds by Chu [3] for spherical geometries to geometries of arbitrary shape. The new bounds are valid for lossless and linearly polarized [4, 6, 7, 16] and elliptically polarized [5] antennas. Moreover, the approach can be used to estimate the performances of many small antennas if the polarizabilities of the antennas are used instead of the circumscribing geometries [4, 7, 16].

The only parameter in the bound that depends on the dynamic properties of the antenna is the generalized (or all spectrum) absorption efficiency, η. This is the generalization of the frequency dependent absorption efficiency analyzed in [1] given by integration of the absorbed and total power, independently, over all wavelengths.

In [4, 6, 7, 16], it is demonstrated that η is close to 1/2 for many small antennas that are connected to a frequency independent resistive load and matched at their first resonance. This is motivated by the minimum scattering property that small matched antennas often possess, *i.e.*, they scatter as much power as they absorb at the resonance frequency giving an absorption efficiency of 1/2 at the resonance frequency [1, 12]. Here, it is shown that small idealized dipole antennas with a dominant first single resonance have an all spectrum absorption efficiency $\eta \lesssim 1/2$. The region around the resonance is minimum scattering but the contributions from regions away from the resonance scatter slightly more power than is absorbed giving a generalized (all spectrum) absorption efficiency close to but less than 1/2.

Minimum scattering is a property that many non electrically small resonant antennas also possess. Numerical simulation results of common antennas, both electrically small and not small, verify the theoretical results.

2 Absorption efficiency

The physical bounds analyzed in [4, 6, 7, 16] are derived for single port, linearly polarized, reciprocal, and lossless antennas with the reflection coefficient $\Gamma(k)$ and the directivity $D(k; \hat{\boldsymbol{k}}, \hat{\boldsymbol{e}})$, where k denotes the free-space wavenumber, $\hat{\boldsymbol{k}}$ the direction, and $\hat{\boldsymbol{e}}$ the electric polarization. The forward scattering sum rule [6] gives the antenna

identity

$$\int_0^\infty \frac{(1-|\Gamma(k)|^2)D(k;\hat{\boldsymbol{k}},\hat{\boldsymbol{e}})}{k^4}\,\mathrm{d}k = \frac{\eta}{2}\left(\hat{\boldsymbol{e}}\cdot\boldsymbol{\gamma}_\mathrm{e}\cdot\hat{\boldsymbol{e}} + (\hat{\boldsymbol{k}}\times\hat{\boldsymbol{e}})\cdot\boldsymbol{\gamma}_\mathrm{m}\cdot(\hat{\boldsymbol{k}}\times\hat{\boldsymbol{e}})\right), \quad (2.1)$$

where $\boldsymbol{\gamma}_\mathrm{e}$ and $\boldsymbol{\gamma}_\mathrm{m}$ are the electro- and magneto-static polarizability dyadics, respectively. The integral (2.1) is bounded in various ways to produce bounds for different applications, *e.g.*, resonant and constant partial-realized gain in [4, 6, 7] and ultra-wide band cases in [16]. The resonant case is applicable for antennas with a dominant first single resonance [7]. It is given by

$$\frac{D(k;\hat{\boldsymbol{k}},\hat{\boldsymbol{e}})}{Q} \leq \frac{\eta k_0^3}{2\pi}\left(\hat{\boldsymbol{e}}\cdot\boldsymbol{\gamma}_\mathrm{e}\cdot\hat{\boldsymbol{e}} + (\hat{\boldsymbol{k}}\times\hat{\boldsymbol{e}})\cdot\boldsymbol{\gamma}_\mathrm{m}\cdot(\hat{\boldsymbol{k}}\times\hat{\boldsymbol{e}})\right), \quad (2.2)$$

where k_0 is the resonance wavenumber and Q denotes the Q-factor at the resonance, *i.e.*, it has the half-power fractional bandwidth $B \approx 2/Q$.

The polarizability dyadics in the right-hand sides of (2.1) and (2.2) are easily determined for the antenna or, as an upper bound, for an arbitrary circumscribing geometry[1] by the solution of the corresponding electro- and magneto-static equations [4, 6, 7, 16]. This leaves the generalized absorption efficiency, η, as the only quantity in the right-hand sides of (2.1) and (2.2) that depends on the dynamic properties of the antenna. It is an all spectrum measure of the absorption and scattering properties of the object, that is defined by

$$\eta = \frac{\int_0^\infty \sigma_\mathrm{a}(k)/k^2\,\mathrm{d}k}{\int_0^\infty \sigma_\mathrm{ext}(k)/k^2\,\mathrm{d}k} = \frac{\int_0^\infty \sigma_\mathrm{a}(2\pi/\lambda)\,\mathrm{d}\lambda}{\int_0^\infty \sigma_\mathrm{ext}(2\pi/\lambda)\,\mathrm{d}\lambda}, \quad (2.3)$$

where $\sigma_\mathrm{ext} = \sigma_\mathrm{a} + \sigma_\mathrm{s}$, σ_a, and σ_s denote the extinction, absorption, and scattering cross sections, respectively and $\lambda = 2\pi/k$ is the wavelength. It is clear that $0 \leq \eta < 1$ for all objects as $\sigma_\mathrm{a} \geq 0$ and $\sigma_\mathrm{s} \geq 0$. In [4, 7], it is observed that $\eta \approx 1/2$ for many small antennas that are matched at a dominant first resonance k_0. This is partly explained by the fact that the absorption efficiency $\sigma_\mathrm{a}(k_0)/\sigma_\mathrm{ext}(k_0) = 1/2$ for minimum scattering antennas, *i.e.*, small single mode antennas absorb and scatter the same amount of power at the resonance frequency [1, 12]. The weighting factor, k^{-2}, in (2.3) emphasizes the dynamics of the antenna for low wavenumbers. Thus, the lower the resonance frequency, the closer η is to $1/2$ as the resonance region will dominate the integrals. As a consequence, the theory derived here is useful if the analyzed resonance has the lowest frequency. The contributions to η in (2.3) away from the resonance are small due to the fact that scattering dominates the behavior of the antenna in the regions where the mismatch is high.

Here, the case with an idealized lossless antenna that radiates an electric dipole mode is considered to explicitly determine η and illustrate how $\sigma_\mathrm{ext}(k)$ and $\sigma_\mathrm{a}(k)$ depend on the wavenumber around the resonance. A spherical dipole mode at the radius a has the impedance [3] $Z_\mathrm{TM} = 1/(\mathrm{j}\omega C) + \mathrm{j}\omega L/(1+\mathrm{j}\omega L/\eta_0)$, where $L = \mu_0 a$, $C = \epsilon_0 a$, $\omega = k\mathrm{c}_0$, the time convention $\mathrm{e}^{\mathrm{j}\omega t}$ is used, and ϵ_0, μ_0, c_0, and η_0 denote the

[1] http://www.mathworks.fr/matlabcentral/fileexchange/26806-antennaq

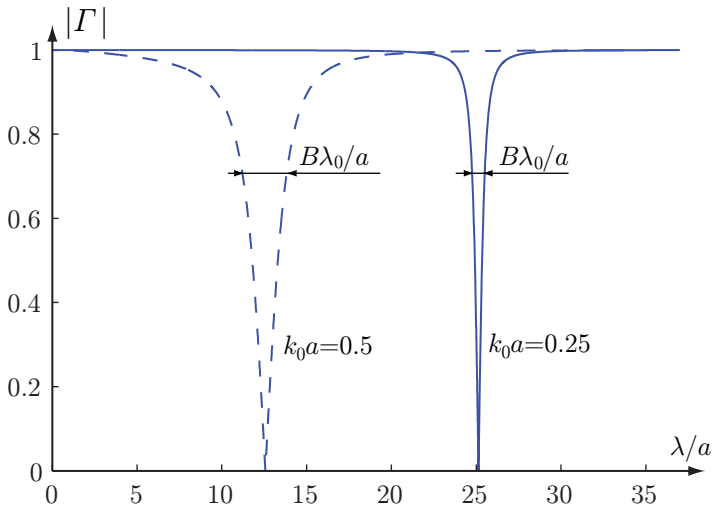

Figure 1: The reflection coefficient of the idealized dipole antenna (2.4) for $k_0a = 1/2$ and $k_0a = 1/4$ with $C = \epsilon_0 a$, $L = \mu_0 a$ and $R_1 = \eta_0$ as function of the normalized wavelength $\lambda/a = 2\pi \mathrm{c}_0/(\omega a)$.

free space permittivity, permeability, speed of light, and impedance, respectively. The impedance is modified by the antenna. We consider an antenna with the input impedance obtained from the impedance of the dipole mode, Z_{TM}, tuned to be resonant at $\omega = \omega_0$ with a lumped inductance L_1, *i.e.*,

$$Z(\omega) = \mathrm{j}\omega L_1 + \frac{1}{\mathrm{j}\omega C} + \frac{\mathrm{j}\omega L}{1 + \mathrm{j}\omega L/R_1}. \tag{2.4}$$

The inductance L_1 is given by $L_1 = 1/(\omega_0^2 C) - L/(1 + \omega_0^2 L^2/\eta_0^2)$, and the radiation resistance at the resonance frequency is $R_0 = Z(\omega_0) = \omega_0^2 L^2 R_1/(R_1^2 + \omega_0^2 L^2)$, and $R_1 = \eta_0$, $L = \mu_0 a$, and $C = \epsilon_0 a$ in the idealized dipole case. The corresponding Q-factor at $\omega = \omega_0$ is determined to $Q = 1/(C^2 L R_1 \omega_0^3) + R_1/(L\omega_0)$ and the reflection coefficient, $\Gamma(\omega) = (Z(\omega) - R_0)/(Z(\omega) + R_0)$, has a single resonance with $\Gamma(\omega_0) = 0$, see Fig. 1. The absorption cross section (or effective antenna aperture) for lossless antennas is given by [15]

$$\sigma_{\mathrm{a}}(k) = D(k)(1 - |\Gamma(k\mathrm{c}_0)|^2)\pi/k^2, \tag{2.5}$$

where $D(k) = 3/2$ in the horizontal plane for the considered dipole mode.

Evaluation of η in (2.3) requires a model of the extinction cross section, $\sigma_{\mathrm{ext}}(k)$, that is consistent with (2.4). Consider a single port antenna with incoming signal u and outgoing signal v. The electromagnetic field is expanded in incoming and outgoing spherical modes with coefficients $\boldsymbol{a}$ and $\boldsymbol{b}$, respectively. This gives the scattering matrix [11]

$$\begin{pmatrix} \Gamma & \boldsymbol{R} \\ \boldsymbol{T} & \mathbf{S} \end{pmatrix} \begin{pmatrix} u \\ \boldsymbol{a} \end{pmatrix} = \begin{pmatrix} v \\ \boldsymbol{b} \end{pmatrix}, \tag{2.6}$$

where Γ is the reflection coefficient, $\boldsymbol{R}$ is an $1 \times \infty$ matrix with elements R_n, $\boldsymbol{T}$ is an $\infty \times 1$ matrix with elements T_n, and $\mathbf{S}$ is an $\infty \times \infty$ matrix with elements S_{mn}.

For simplicity, order the modes such that the idealized dipole antenna radiates the first mode, *i.e.*, $R_n = T_n = 0$ for $n > 1$. Conservation of energy shows that the amplitudes of the reflection coefficient and the scattering coefficient, S_{11}, are identical in this case, *i.e.*,

$$|\Gamma(k\mathrm{c}_0)| = |S_{11}(k)| \tag{2.7}$$

for $k \in \mathbb{R}$. Moreover, the scattering matrix is non-causal, *i.e.*, it increases as $\mathrm{e}^{2\mathrm{j}ka}$ as $k \to \infty$ with $|\arg(\mathrm{j}k)| < \pi/2 - \alpha$, for some $\alpha > 0$ where a denotes the radius of the smallest circumscribing sphere, see [9, 14]. As the amplitude of S_{11} is determined by the reflection coefficient (2.7) they can only differ by a function that has unit magnitude for $k \in \mathbb{R}$. Using rational functions, *i.e.*, Blaschke products [14], gives the model

$$S_{11}(k) = \mathrm{e}^{2\mathrm{j}ka} \frac{Z(k\mathrm{c}_0) - R_0}{Z(k\mathrm{c}_0) + R_0} \prod_n \frac{k_n - k}{k_n^* - k}, \tag{2.8}$$

where k_n denote the zeros of S_{11} in $\mathrm{Re}\{\mathrm{j}k\} > 0$.

The extinction cross section is often expressed in the transition matrix. It is related to the S-matrix in (2.6), $\mathbf{S}$, via $\mathcal{T}_{mn} = (S_{mn} - 1)/2$. Consider an idealized dipole antenna that is resonant for $k_0 a \ll 1$. The scattering from higher order modes is negligible for $k_0 a \ll 1$ so the extinction cross section is well approximated with the dipole mode in this region. The extinction cross section from the dipole mode is hence approximated by

$$\sigma_{\mathrm{ext}}(k) \approx -\frac{6\pi\,\mathrm{Re}\,\{\mathcal{T}_{11}(k)\}}{k^2} \quad \text{and } \sigma_{\mathrm{s}}(k) \approx \frac{6\pi|\mathcal{T}_{11}(k)|^2}{k^2}, \tag{2.9}$$

where $\mathcal{T}_{11}$ denotes the diagonal dipole element of the transition matrix [14]. Consider the simplest possible case with a single zero k_1. The value of k_1 is determined by (2.8) and (2.9) inserted into the low-frequency expansions [13] $\sigma_{\mathrm{ext}}(k) = \mathcal{O}(k^2)$ and $\sigma_{\mathrm{s}}(k) = \mathcal{O}(k^4)$ as $k \to 0$. This shows that $k_1 = \mathrm{j}/(a - CR_0\mathrm{c}_0)$, giving the model

$$S_{11}(k) = \mathrm{e}^{2\mathrm{j}ka}\, \frac{Z(k\mathrm{c}_0) - R_0}{Z(k\mathrm{c}_0) + R_0}\, \frac{1 - \mathrm{j}k(a - CR_0\mathrm{c}_0)}{1 + \mathrm{j}k(a - CR_0\mathrm{c}_0)}. \tag{2.10}$$

The cross sections σ_{ext}, σ_{a}, and σ_{s} are depicted in Fig. 2 for the same cases as in Fig. 1. It is observed that the areas under the curves are concentrated to the resonances and that $\sigma_{\mathrm{a}}(k) \approx \sigma_{\mathrm{s}}(k)$ around the resonances for $k_0 a = 0.25$. For minimum scattering, $\mathrm{Re}\,\{\mathcal{T}_{11}(k)\} = -1/2$ in (2.9), we obtain the envelope $\sigma_{\mathrm{ext}}(k)/a^2 \approx 3\pi/k^2a^2 = 3\lambda^2/4\pi a^2$, also plotted in Fig. 2. The more dominant a resonance, the closer the obtained value of the extinction cross section is to this envelope at the resonance frequency.

The generalized (all-spectrum) absorption efficiency (2.3) for the idealized dipole is finally determined by

$$\eta = \frac{\int_0^\infty \frac{(1-|\Gamma(k)|^2)D\pi}{k^4}\,\mathrm{d}k}{\int_0^\infty \frac{\sigma_{\mathrm{ext}}(k)}{k^2}\,\mathrm{d}k} \approx \frac{\int_0^\infty \frac{1-|\Gamma(k)|^2}{k^4}\,\mathrm{d}k}{-4\int_0^\infty \frac{\mathrm{Re}\{\mathcal{T}_{11}(k)\}}{k^4}\,\mathrm{d}k}. \tag{2.11}$$

In Fig. 3, the generalized absorption efficiency η is evaluated for the idealized dipole model (2.4) and (2.10) as well as various other parameter values on C, L, and R_1.

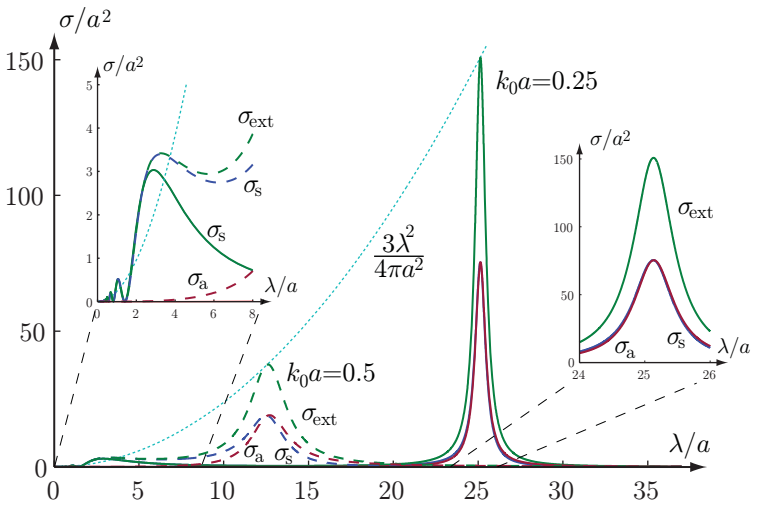

Figure 2: The extinction, $\sigma_{\rm ext}$, absorption, $\sigma_{\rm a}$, and scattering, $\sigma_{\rm s}$, cross sections for the idealized dipole antenna (2.4), depicted in Fig. 1, and (2.10) as function of the normalized wavelength $\lambda/a = 2\pi/(ka)$.

It is observed that $\eta \lesssim 1/2$ for $k_0 a \ll 1$. The deviation from $1/2$ is due to the region with small $\sigma_{\rm s}$ but negligible $\sigma_{\rm a}$ for $\lambda/a < 8$ as seen in Fig. 2.

The particular impedance (2.4) is not crucial for this result. It is sufficient that the contributions to the integrals in (2.3) are dominated by the region around the resonance k_0 and that $\sigma_{\rm a}$ and $\sigma_{\rm ext}$ have similar bandwidths and shapes. It is common to assume antennas with a single resonance structure [8] to relate the bandwidth with the antenna Q. Similarly, assume that the transition matrix element $\mathcal{T}_{11}(k)$ has a single resonance at k_0 and is minimum scattering, *i.e.*, $S_{11}(k_0) = 0$ implying $\mathcal{T}_{11}(k_0) = -1/2$. The resonance model has complex valued poles at $k \approx \pm k_0$ and the shape of the classical Lorentz or resonance circuit [8, 14] around the resonance, *i.e.*,

$$\mathcal{T}_{11}(k) = \frac{-1/2}{1 + \frac{\rm j}{\nu}\left(\frac{k}{k_0} - \frac{k_0}{k}\right)} = \frac{-{\rm j}\nu k/(2k_0)}{1 - k^2/k_0^2 + {\rm j}\nu k/k_0} \tag{2.12}$$

with $0 < \nu \ll 1$. It satisfies

$$-\,{\rm Re}\left\{\mathcal{T}_{11}(k)\right\} = \frac{1/2}{1 + \frac{1}{\nu^2}\left(\frac{k}{k_0} - \frac{k_0}{k}\right)^2} = 2|\mathcal{T}_{11}(k)|^2 \tag{2.13}$$

for all $k \in \mathbb{R}$ showing that $\sigma_{\rm ext}(k) = 2\sigma_{\rm s}(k) = 2\sigma_{\rm a}(k)$ around the resonance wavenumber, see the $k_0 a = 1/4$ case in Fig. 2. For antennas with negligible $\sigma_{\rm a}$ away from the resonance, *e.g.*, the dipole model (2.4), the $\sigma_{\rm ext} \approx \sigma_{\rm s}$ contribution to the integral (2.3) away from the resonance gives $\eta \lesssim 1/2$.

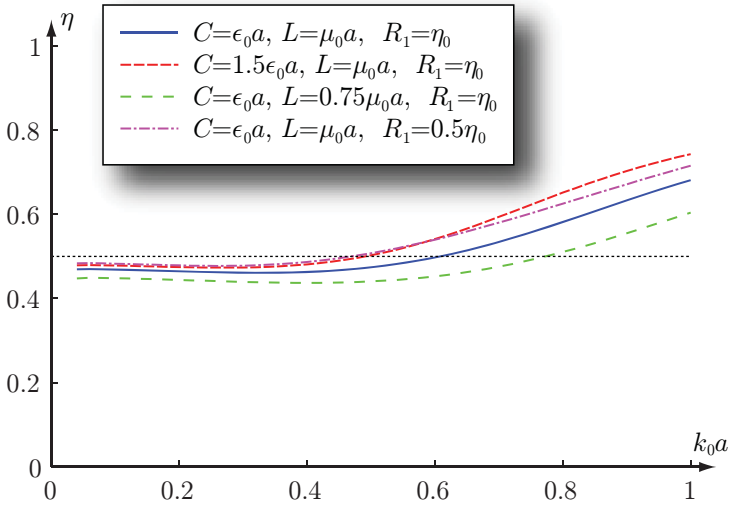

Figure 3: The generalized absorption efficiency for the idealized dipole antenna (2.4) and (2.10) and various values of C, L, and R_1 as function of the normalized resonance wavenumber $k_0 a$.

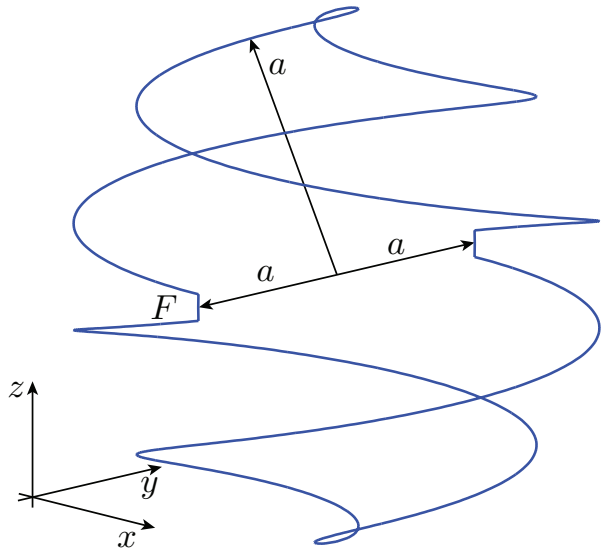

Figure 4: Geometry of the two arm spherical helix with circumscribing sphere radius $a = 62\,\mathrm{mm}$ and wire radius $R_\mathrm{w} = 2\,\mathrm{mm}$.

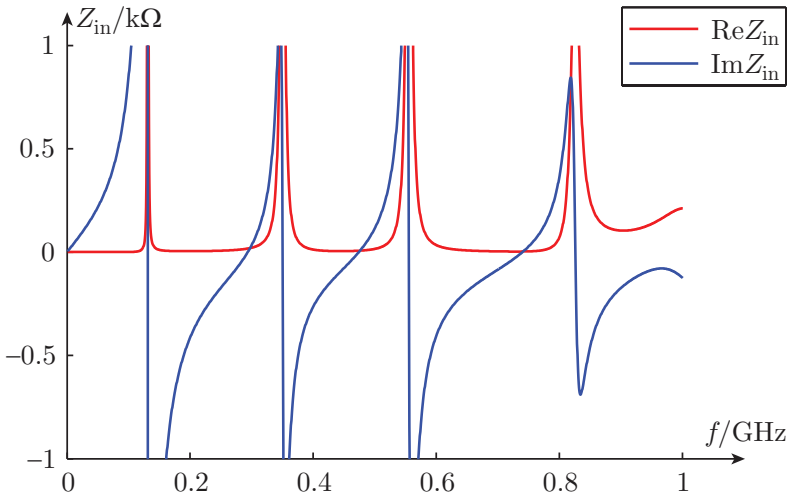

Figure 5: Input impedance of the spherical helix depicted in Fig. 4.

3 Numerical Examples

The above theoretical results have been analyzed for a number of geometries by numerical simulations; the numerical results show very good agreement with the theory. For each of the examples the approach was the same; first we started with the design and simulation of a radiating structure using the Method of Moments (MoM) simulator in Efield[2]. Then the radiation resistance at the first resonance was used as a load at the feeding point in a forward scattering simulation, performed using the same software. The results of the antenna and scattering simulations have been used to numerically compute the theoretical parameters using Matlab. Note that not all the available digits are presented in the text as the numerical accuracy does not justify them. However the formulas are computed without truncation.

3.1 Folded Spherical Helix – $D = 1.5$, $k_0 a = 0.38$

We first describe the results for the folded spherical helix [2] depicted in Fig. 4. It comprises a closed loop of perfectly electric conducting wire of radius $R_{\text{w}} = 2\,\text{mm}$ that is folded on the surface of a sphere of radius 58 mm thus obtaining a structure with the radius of the smallest circumscribing sphere $a = 62\,\text{mm}$. The structure has two arms of equal length (approximately $l_{\text{a}} = 646\,\text{mm}$) symmetric with respect to the z axis.

The first step in the analysis is to simulate this structure with Efield. The antenna parameters are determined with an ideal voltage source connected at point F (see Fig. 4). The resulting input impedance is plotted in Fig. 5. The first interesting resonance from a practical point of view appears around 294 MHz with a radiation resistance of 17 Ω. It is this resonance that is used to illustrate the physical bounds

[2] www.efieldsolutions.com

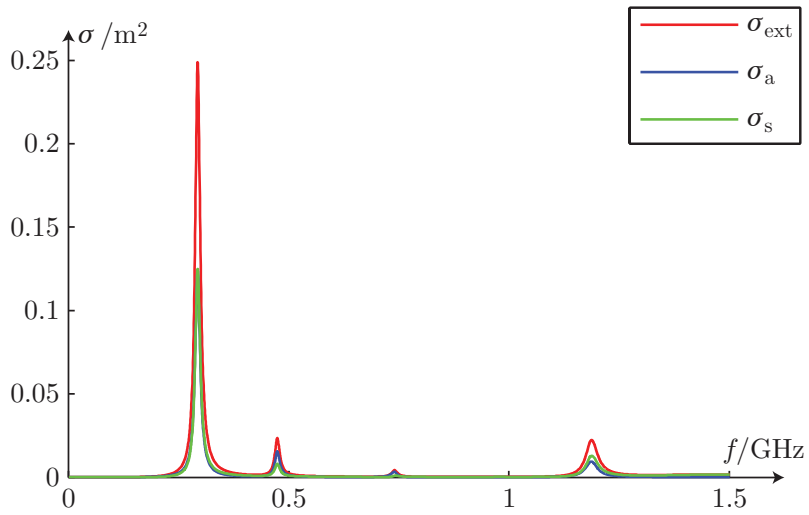

Figure 6: Extinction, absorption and scattering cross sections of the spherical helix depicted in Fig. 4.

in [4, 6, 7, 16]. At this frequency the antenna radiates a z dipole type pattern. First we compute the $D/(Qk_0^3a^3)$ value using the simulation data from Efield and the method proposed in [8, 18] to approximate the Q factor. The computed values $D = 1.5$, $Q = 43$ and $k_0a = 0.38$ result in the quotient $D/(Qk_0^3a^3) = 0.63$.

The second step is to evaluate the right hand side in (2.2). Here, the polarizability dyadics reduce to the high contrast polarizability dyadic of the perfect electric conductor which is computed using a MoM algorithm (see *e.g.*, [4]) that solves the electrostatic problem associated with the wire geometry. With $\hat{\boldsymbol{e}} = \hat{\boldsymbol{z}}$ and only high contrast electric material present $\hat{\boldsymbol{e}} \cdot \boldsymbol{\gamma}_\mathrm{e} \cdot \hat{\boldsymbol{e}} + (\hat{\boldsymbol{k}} \times \hat{\boldsymbol{e}}) \cdot \boldsymbol{\gamma}_\mathrm{m} \cdot (\hat{\boldsymbol{k}} \times \hat{\boldsymbol{e}})$ evaluates to:

$$\hat{\boldsymbol{z}} \cdot \boldsymbol{\gamma}_\infty \cdot \hat{\boldsymbol{z}} = 2 \cdot 10^{-3}\,\mathrm{m}^3.$$

The generalized absorption efficiency is computed from the Efield simulation data with (2.3) and the definitions of absorption and extinction cross sections from [7, 17]. After an integration of 5999 absorption and extinction cross sections samples taken equidistantly between 1 MHz and 3 GHz (see Fig. 6) we obtain $\eta \approx 0.51$ and write:

$$\frac{D}{Qk_0^3a^3} \approx 0.63 \leq 0.67 \approx \frac{\eta}{2\pi a^3}\,(\hat{\boldsymbol{z}} \cdot \boldsymbol{\gamma}_\infty \cdot \hat{\boldsymbol{z}})\,.$$

This is a true relation showing that the antenna performs close to the D/Q bound of the wire structure.

Moreover, the integrated extinction cross section is related to the polarizability of the structure, as stated in [17] *i.e.*,

$$\frac{2}{\pi}\int_0^\infty \frac{\sigma_\mathrm{ext}(k)}{k^2}\,\mathrm{d}k = \frac{1}{\pi^2}\int_0^\infty \sigma_\mathrm{ext}(\lambda)\,\mathrm{d}\lambda \approx 1.99 \cdot 10^{-3}\,\mathrm{m}^3$$

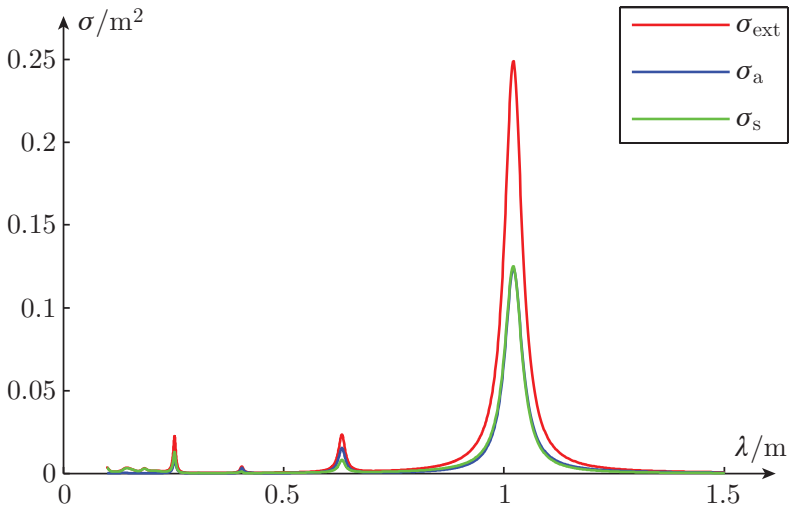

Figure 7: Extinction, absorption and scattering cross sections of the spherical helix depicted in Fig. 4 as function of wavelength, $\lambda = 2\pi/k = \mathrm{c}_0/f$.

which is approximately 1% away from the polarizability determined from the MoM simulation. This deviation can be attributed to the high frequecies (low wavelengths) which are missing in Fig. 7. The cross sections should show one dominant resonance and asymptotically tend to 0 for low frequencies.

The physical bounds in (2.2) create a link between the dynamic properties of the radiating structure and its static properties described by the electric and magnetic polarizability dyadics. Because many common antennas have a generalized absorption efficiency of approximately 1/2 obtaining the bounds for an antenna reduces to a static problem of computing the polarizability dyadics for the geometry, which is easily solved using a Method of Moments algorithm.

It is very important to distinguish the geometry of the radiating structure from its smallest circumscribing sphere. The antenna can be optimized in the limit given by its own polarizability, *e.g.*, the smallest circumscribing sphere of the helix in Fig. 4 has the radius $a = 62\,\mathrm{mm}$, which gives $\hat{\boldsymbol{z}} \cdot \boldsymbol{\gamma}_\infty \cdot \hat{\boldsymbol{z}} = 4\pi a^3 \approx 3 \cdot 10^{-3}\,\mathrm{m}^3$ thus the maximum attainable value for the D/Q quotient is: $D/(Qk_0^3a^3) \leq 1$, whereas the wire structure simulated here has a maximum attainable value $D/(Qk_0^3a^3) \leq 0.67$. The presence of the $(k_0a)^3$ term allows radiating structures to be directly compared even though they do not have the same size. It can be stated that the wire structure of the helix in Fig. 4 can only reach 67% of the best attainable performance of an antenna circumscribed by a sphere with equal radius. Hence, it is neccesary to use a structure with high polarizability to improve the performance, *e.g.*, the polarizability of the spherical helix increases with the number of arms and with the wire radius.

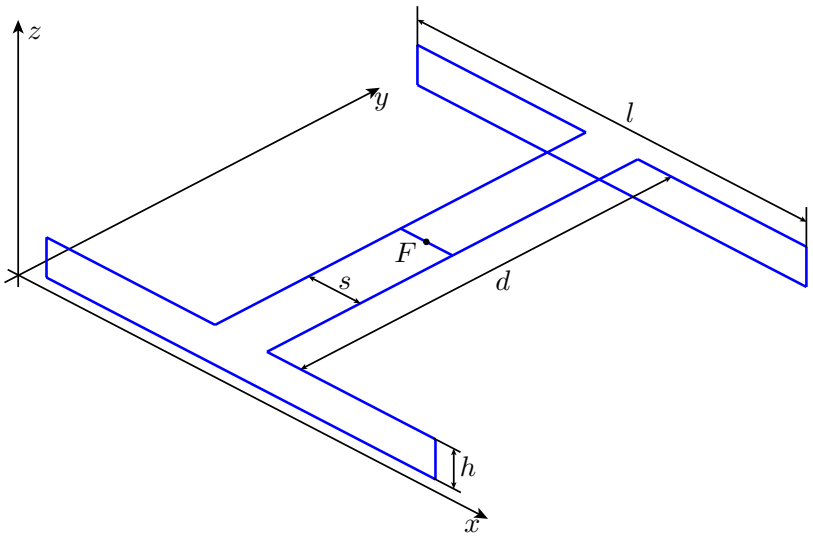

Figure 8: Two element array of folded dipoles with $l = 492.9\,\text{mm}$ and $d = 470\,\text{mm}$.

3.2 Folded Dipole Array – $D = 2.6$, $k_0 a = 1.7$

The second considered structure is a folded dipole array [10]. The dimensions in Fig. 8 are the following: $l = 492.9\,\text{mm}$, $d = 470\,\text{mm}$, $h = 40\,\text{mm}$ and $s = 65.8\,\text{mm}$. The structure is assumed to be fed at point F with an ideal voltage source. All wires have a radius of $R_\text{w} = 4\,\text{mm}$ thus simulating one possible realization of a simple and common array design using the same type of conductor for all the elements. The smallest circumscribing sphere has the radius $a = 347\,\text{mm}$.

First we simulate the structure in transmission in order to obtain the impedance behavior in the frequency range of interest, see Fig. 9. The first resonance with practical relevance is close to 233 MHz and, at this frequency the antenna has an input impedance of $59\,\Omega$. We shall illustrate the bounds using the characteristics of the structure at this frequency. The far field radiation pattern at this resonance consists of two linearly polarized ($\hat{\boldsymbol{x}}$-direction) pencil beams in the broad sides, with a maximum directivity $D = 2.6$. The quality factor of this resonance is $Q = 4.2$ and with $k_0 a = 1.7$ we obtain the quotient $D/(Qk_0^3 a^3) = 0.13$.

The high contrast polarizability for $\hat{\boldsymbol{e}} = \hat{\boldsymbol{x}}$ polarization has the value $\gamma_{\infty,11} = 67.4 \cdot 10^{-3}\,\text{m}^3$. We note here that the structure is also highly polarizable on the $\hat{\boldsymbol{y}}$-direction but the $\hat{\boldsymbol{y}}$-polarization does not contribute to the radiation because of the choice of feeding.

We now turn to the analysis of the cross sections and use 5999 absorption and extinction cross section samples from equidistantly spaced frequencies between 1 MHz and 3 GHz. The first and dominating resonance is shown in Fig. 10. The array has a two band behavior; in either of the two bands it approximately absorbs as much energy as it scatters. Besides these two resonances there is another scattering resonance which contributes to the generalized absorption efficiency. By comparing Fig. 6 with Fig. 10 we expect to have differences between the two generalized ab-

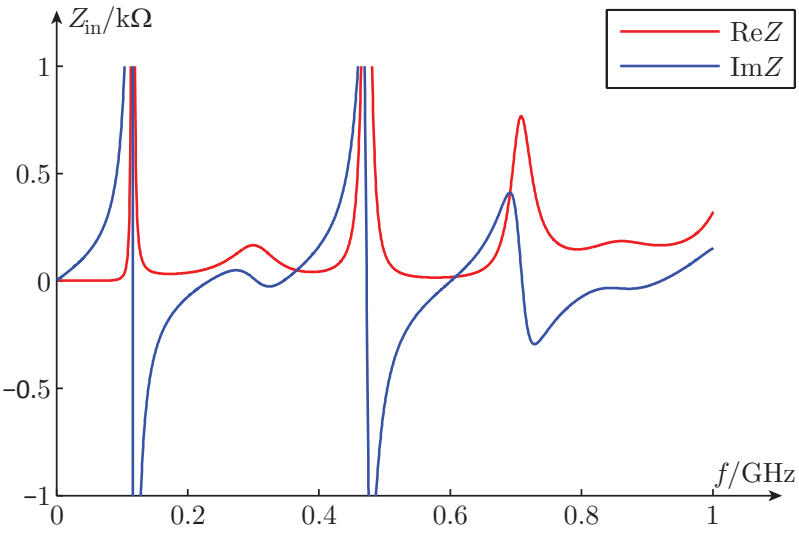

Figure 9: Input impedance of the array depicted in Fig. 8.

sorption efficiencies but in fact $\eta \approx 0.48$. The reason for the small deviation is the presence of the second resonance very close to the first one, and with comparable values of the radiation resistance.

Gathering the results, we rewrite (2.2) in numbers as: $0.13 \leq 0.13$ thus making this array a structure that is close to the optimal D/Q performance of the wire structure. The perfect matching is explained by the deviation of the structure from the assumed models for the Q-factor ($Q \gg 1$) and the first single and dominant resonance. Compared with a smallest circumscribing sphere, the array only reaches 13% of its D/Q performance. For evaluating the reliability of the generalized absorption efficiency we integrate the extinction cross section over the wavelength and obtain the value $66.8{\cdot}10^{-3}\,\text{m}^3$ which is less than 1% from the previous $\gamma_{\infty,11} = 67.4{\cdot}10^{-3}\,\text{m}^3$; so the frequency interval is well chosen as to not significantly deviate the resulted η from its correct value.

3.3 Meanderline – $D = 1.6$, $k_0 a = 1.14$

We now analyze a planar meander line antenna depicted in Fig. 11. The notations follow [7]: l_1 is the "long" and l_2 is the "short" dimension of the antenna, w is the metal width and h is the base meander height. We only analyze situations where the $\boldsymbol{E}$ field is polarized along l_1.

First we simulate the antenna in transmission and use for this purpose an ideal voltage source distributed along line F. The impedance behavior is shown in Fig. 12. At low frequencies the antenna is a resonating structure with the first resonance approximately at frequency 322 MHz; at high frequencies the input impedance shows very little variations both in the real and imaginary parts – ultra wide band behavior. The radiated pattern shows an almost dipole mode radiation at 322 MHz polarized along y with a directivity $D = 1.6$ and a radiation resistance of approximately $45\,\Omega$.

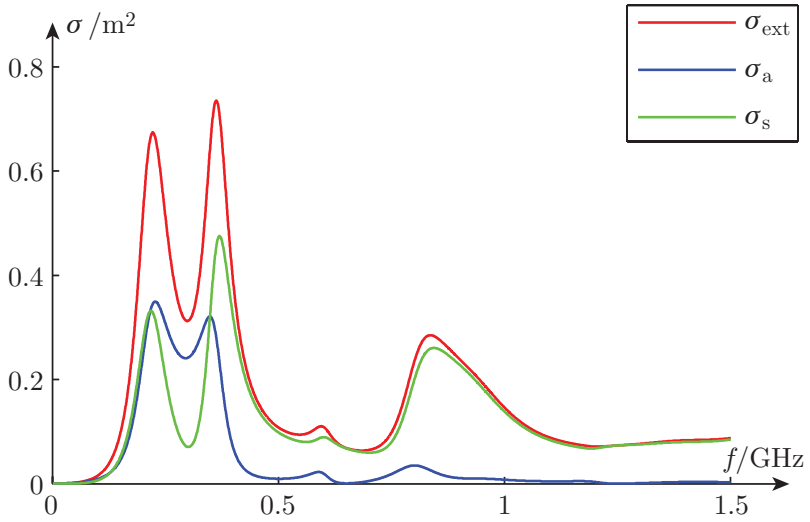

Figure 10: Extinction, absorption and scattering cross sections of the array depicted in Fig. 8.

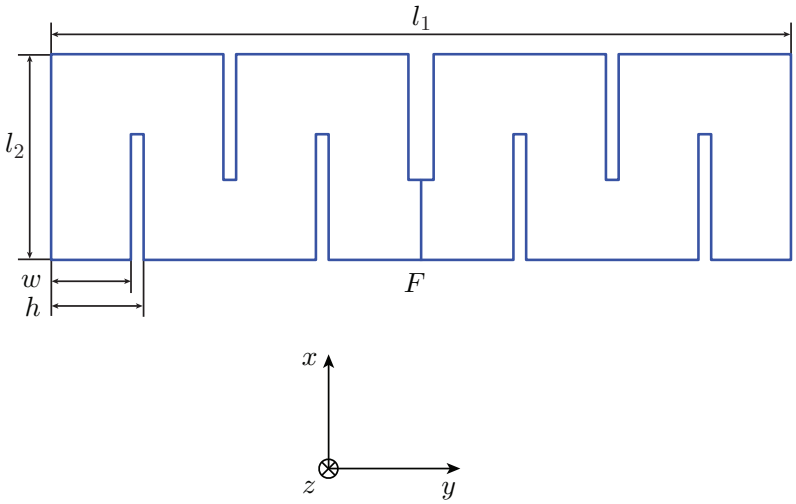

Figure 11: Planar meanderline antenna: $l_1 = 324\,\mathrm{mm}$, $l_2 = 90\,\mathrm{mm}$, $w = 35\,\mathrm{mm}$, $h = 40.5\,\mathrm{mm}$.

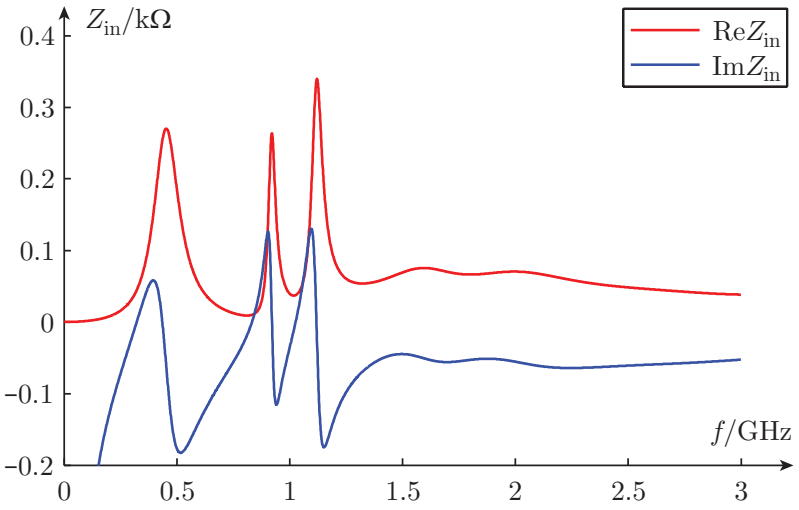

Figure 12: Input impedance of the antenna depicted in Fig. 11.

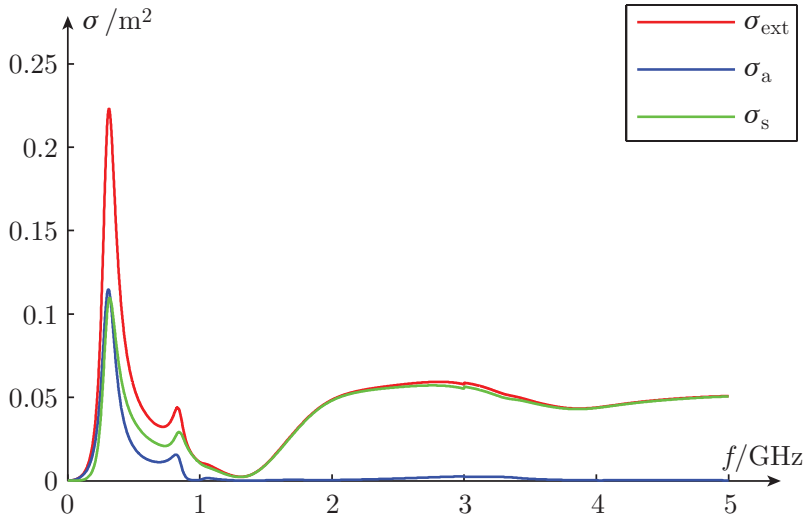

Figure 13: Extinction, absorption and scattering cross sections of the antenna depicted in Fig. 11.

Small variations in the directivity affect the omnidirectionality with the maximum directivity obtained on a direction slightly deviated from z ($\theta \approx 10\,^\circ$, $\phi = 0\,^\circ$). The other parameters that characterize radiation at 322 MHz are: $Q = 4.4$ and $k_0 a = 1.14$ and the quotient $D/(Qk_0^3 a^3) = 0.247$.

Next, we use a MoM code to compute the static high contrast electric polarizability dyadic of the structure and obtain: $\gamma_{\infty,22} = 14.667 \cdot 10^{-3}\,\mathrm{m}^3$. This value serves as a reference for the integrated extinction cross section and thus as a reliability figure for the generalized absorption efficiency.

The last step in the analysis consists of a forward scattering simulation that provides data for the cross sections of the structure. We use the same value for the feed load as the radiation resistance (approximately 45 Ω). The structure is excited with a plane wave impinging the structure from the direction of the maximum directivity (here $\theta = 10\,^\circ$, $\phi = 0\,^\circ$). In total 4000 frequency samples were simulated between 1 MHz and 5 GHz, equally spaced at 1 MHz up to 3 GHz and at 2 MHz above. Fig. 13 shows that this antenna does not have a single dominant resonance behavior; this fact is reflected in the following figures. The generalized absorption efficiency is 0.52 and the integrated extinction cross section has a value of $14.204 \cdot 10^{-3}\,\mathrm{m}^3$ which deviates less than 3.3% from $\gamma_{\infty,22} = 14.667 \cdot 10^{-3}\,\mathrm{m}^3$.

We rewrite (2.2) in numbers as: $0.247 \leq 0.248$. This structure performs close to the optimal performance of the planar antenna. Compared to the smallest circumscribing sphere, this meanderline antenna achieves approximately 25% of the performance of the optimal sphere structure.

The bounds (2.2) do not depend on the choice of direction of radiation and polarization *i.e.*, $\hat{\boldsymbol{k}}$ and $\hat{\boldsymbol{e}}$. The previous results considered the situation where $\hat{\boldsymbol{k}}$ was the direction of the maximum radiation and η was computed based on a scattering simulation data with a plane wave impinging from the same direction (see [7]). The polarization of the wave was the polarization most favored by the structure.

Table 1 illustrates the bounds (2.2) for different radiation/incidence directions. There aren't so many choices for these directions because the structure radiates almost omnidirectionally. The difference from the previous approach is that scattering simulation uses a plane wave impinging from the directions given by (θ, ϕ). Two things can be checked in Table 1: first $\frac{D}{Qk_0^3 a^3} \leq \frac{\eta\gamma}{2\pi a^3}$, in agreement with (2.2), and second, the integrated extinction cross section (IECS) is less than or equal to γ where $\gamma = \hat{\boldsymbol{e}} \cdot \boldsymbol{\gamma}_\infty \cdot \hat{\boldsymbol{e}}$ is the electric polarizability corresponding to the chosen incidence. The figures are in good agreement, showing, as before, that the antenna performs close to the optimal performance of the planar antenna. The differences in the integrated extinction cross section come from a limited number of samples, only 3000, 1 MHz apart, from 1 MHz to 3 GHz.

3.4 Meanderline – $D = 1.6$, $k_0 a = 0.73$

This meanderline structure is a modified version of the previous design that improves radiation resistance. To achieve this, the antenna is featured with a loop in the feeding area, see Fig. 14.

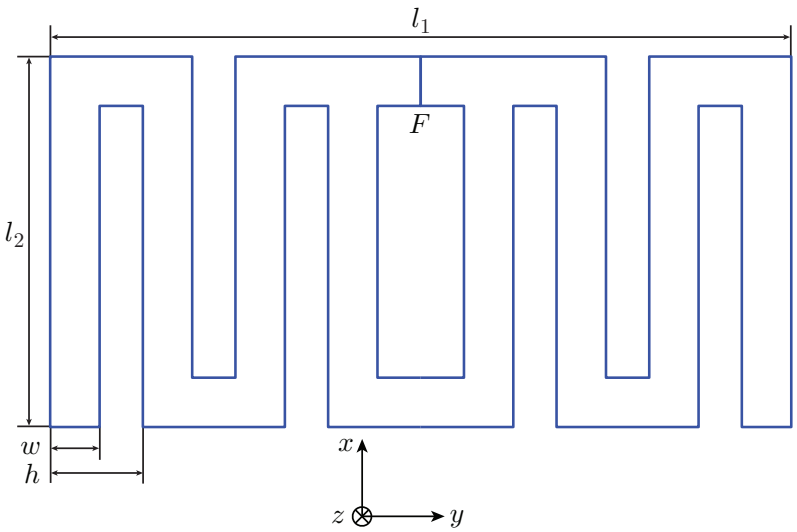

Figure 14: Planar meanderline antenna: $l_1 = 300\,\text{mm}$, $l_2 = 150\,\text{mm}$, $w = 20\,\text{mm}$, $h = 37.5\,\text{mm}$.

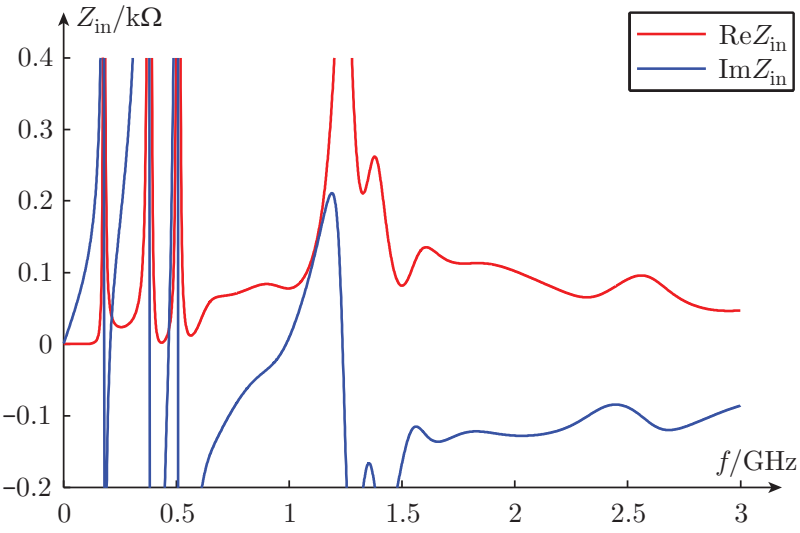

Figure 15: Input impedance of the antenna depicted in Fig. 14.

$\theta[^\circ]$	$\phi[^\circ]$	D	Q	k_0a	$\frac{D}{Qk_0^3a^3}$	$\frac{\eta\gamma}{2\pi a^3}$	η	$\frac{\gamma}{a^3}$	$\frac{\text{IECS}}{a^3}$
0	90	1.6	4.4	1.14	0.247	0.260	0.53	3.09	2.95
20	90	1.4	4.4	1.14	0.211	0.222	0.51	2.72	2.60
40	90	0.8	4.4	1.14	0.129	0.139	0.48	1.81	1.71
60	90	0.3	4.4	1.14	0.050	0.057	0.47	0.77	0.72

Table 1: Numerical results for the antenna depicted in Fig. 11.

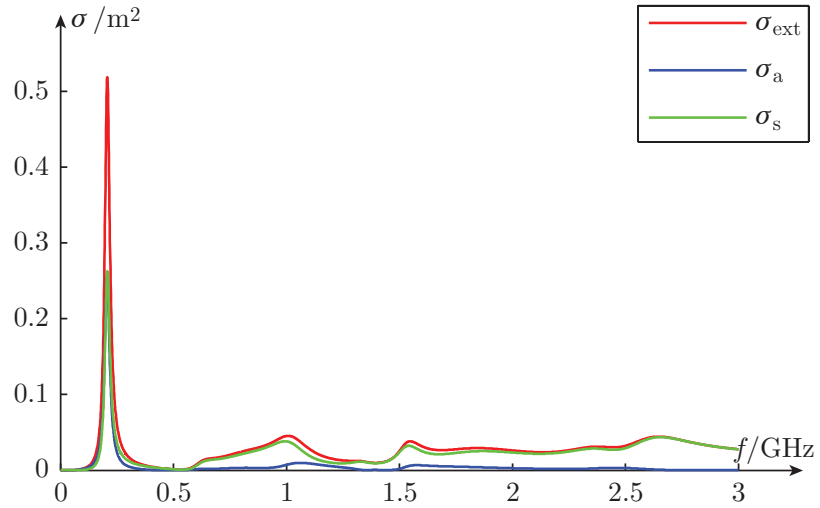

Figure 16: Extinction, absorption and scattering cross sections of the antenna depicted in Fig. 14.

We start by analyzing the most interesting and useful radiation/scattering situation where the directivity is analyzed on the direction of maximum radiation. We simulate the structure in transmission exciting it with a voltage source distributed along line F. The impedance behavior is shown in Fig. 15. The structure is strongly resonating in the low frequencies and shows some irregular behavior in the high frequencies. The first resonance is at a frequency of approximately 208 MHz for which the radiated field shows an almost omnidirectional pattern with small variations in the directivity. Maximum directivity $D = 1.58$ is obtained for a direction with $\theta \approx 20^\circ$ and $\phi = 0^\circ$. Radiation resistance is approximately $48\,\Omega$, $Q = 16$, $k_0a = 0.73$ and the quotient $D/(Qk_0^3a^3) = 0.258$.

The MoM code gives a value for the polarizability in the direction l_1, $\gamma_{\infty,22} = 16.357 \cdot 10^{-3}\,\text{m}^3$. This figure is used further in the analysis as a reference for the integrated extinction cross section and as a reliability factor for the generalized absorption efficiency.

In the forward scattering simulation we use a load along the feeding line with the same value as the radiation resistance and excite the antenna with a plane wave impinging from the direction $\theta = 20^\circ$ and $\phi = 0^\circ$. Cross sections are computed

from 3000 frequency samples of the far field, uniformly distributed between 1 MHz and 3 GHz (see Fig. 16). Integrating these variables gives a value $\eta = 0.48$. The integrated extinction cross section has a value of $15.867 \cdot 10^{-3}\,\mathrm{m}^3$ which is 3% away from $\gamma_{\infty,22} = 16.357 \cdot 10^{-3}\,\mathrm{m}^3$.

We rewrite the bounds (2.2) with numbers as: $0.258 \leq 0.267$. This structure performs close to the optimal planar structure (but not as close as the previous antenna). Compared to the smallest circumscribing sphere this structure is comparable with the previous one achieving, at most, approximately 27% of the performance of the optimal sphere structure.

The structure is considered in other directions of radiation/scattering and the results are shown in Table 2. The conditions are the same as in the previous section.

$\theta[^\circ]$	$\phi[^\circ]$	D	Q	$k_0 a$	$\frac{D}{Qk_0^3a^3}$	$\frac{\eta\gamma}{2\pi a^3}$	η	$\frac{\gamma}{a^3}$	$\frac{\mathrm{IECS}}{a^3}$
0	90	1.6	16	0.73	0.256	0.273	0.49	3.47	3.36
20	90	1.4	16	0.73	0.224	0.238	0.49	3.06	2.97
40	90	0.9	16	0.73	0.144	0.154	0.48	2.03	1.97
60	90	0.4	16	0.73	0.059	0.064	0.47	0.87	0.83

Table 2: Numerical results for the antenna depicted in Fig. 14.

3.5 Other Structures

A number of other structures have been analyzed and the results are gathered in Table 3. The first eight rows in the table correspond to planar geometries circumscribed by different $l_1 \times l_2$ rectangles with l_1/l_2 respectively equal to: 500, 100, 25, 9, 3.6, 2, 1 and 0.5. The polarization is always directed along l_1, the long dimension of the antenna in most of the cases. The two meander type antennas on rows five and six are described in 3.3 and 3.4, respectively. The ninth and tenth rows correspond to the structures described respectively in 3.1 and 3.2.

The eleventh and twelfth rows correspond to four element arrays fed in phase to obtain two broadside pencil shaped lobes. For the first one the elements are represented by simple dipoles of length $l = 500\,\mathrm{mm}$ spaced at $d = 500\,\mathrm{mm}$ and wire radius $R_w = 1\,\mathrm{mm}$ and for the second the elements are folded dipoles with length $l = 502\,\mathrm{mm}$ and height $h = 6\,\mathrm{mm}$ spaced at $d = 470\,\mathrm{mm}$ and wire radius $R_w = 2\,\mathrm{mm}$. Both structures are fed through transmission lines made from the same wire as the radiating elements.

The last line corresponds to a two element array, each element being a Yagi antenna with a reflector ($l_r = 510\,\mathrm{mm}$), driven element ($l_f = 500\,\mathrm{mm}$) and director ($l_d = 420\,\mathrm{mm}$) spaced at $l_s = 200\,\mathrm{mm}$. The distance between the elements in the array is $d = 470\,\mathrm{mm}$ and the wire radius is $R_w = 5\,\mathrm{mm}$. Feeding is realized with a transmission line made from the same wire as the elements.

It must be noted that the table contains some examples that fail to obey the resonance model and thus cannot be characterized properly by their static properties.

In this category fall loop structures, *e.g.*, folded dipole with aspect ratio of 9 and the loops with aspect ratio of 1 and 0.5. The quality factor for these structures is very small due to very close first and second resonances. There are two structures that show a low Q but still obey the bounds, namely the folded dipole arrays. In these cases the structures are not thoroughly designed yielding lower performances at their first resonances.

	D	Q	k_0a	$\frac{D}{Qk_0^3a^3}$	$\frac{\eta\gamma}{2\pi a^3}$	η	$\frac{\gamma}{a^3}$	$\frac{\text{IECS}}{a^3}$
	1.64	8	1.51	0.056	0.058	0.51	0.705	0.693
	1.64	6	1.49	0.078	0.079	0.52	0.962	0.955
	1.63	6	1.43	0.088	0.090	0.52	1.087	1.071
	1.64	3	1.44	0.173	0.155	0.50	1.944	1.901
	1.55	18	0.72	0.231	0.244	0.52	2.972	2.801
	1.54	57	0.48	0.246	0.287	0.54	3.309	3.202
	2.23	5	1.31	0.211	0.200	0.52	2.429	2.401
	3.04	5	1.92	0.095	0.089	0.51	1.085	1.073
	1.50	43	0.38	0.631	0.728	0.51	9.339	8.894
	2.63	4	1.69	0.130	0.130	0.48	1.698	1.683
	6.15	20	3.84	0.005	0.008	0.42	0.116	0.114
	6.30	7	4.08	0.013	0.013	0.41	0.194	0.189
	3.21	17	1.72	0.036	0.042	0.14	1.897	1.832

Table 3: Numerical results of the antennas in 3.5.

4 Conclusions

We demonstrate that $\eta \lesssim 1/2$ for small, $k_0a \ll 1$, idealized dipole antennas and for minimum scattering antennas with a dominant first single resonance. As observed in [4, 7] this is also valid for several antennas that are of the order $k_0a \approx 1$. Here, it is important to realize that the identity (2.1) is not restricted to electrically small antennas and that η in general cannot be replaced by 1/2. Many antennas, *e.g.*,

Yagi-Uda and reflector antennas have $\eta \ll 1/2$ and some, *e.g.*, the spiral antenna in [16], have $\eta > 1/2$.

Acknowledgments

The support of the Swedish research council and the discussions with Anders Derneryd are gratefully acknowledged.

References

[1] J. B. Andersen and A. Frandsen. Absorption efficiency of receiving antennas. *IEEE Trans. Antennas Propagat.*, **53**(9), 2843–2849, 2005.

[2] S. R. Best. The radiation properties of electrically small folded spherical helix antennas. *IEEE Trans. Antennas Propagat.*, **52**(4), 953–960, 2004.

[3] L. J. Chu. Physical limitations of omni-directional antennas. *Appl. Phys.*, **19**, 1163–1175, 1948.

[4] A. Derneryd, M. Gustafsson, G. Kristensson, and C. Sohl. Application of gain-bandwidth bounds on loaded dipoles. *IET Microwaves, Antennas & Propagation*, **3**(6), 959–966, 2009.

[5] M. Gustafsson and C. Sohl. New physical bounds on elliptically polarized antennas. In *Proceedings of the Third European Conference on Antennas and Propagation*, pages 400–402, Berlin, Germany, March 23–27 2009. The Institution of Engineering and Technology.

[6] M. Gustafsson, C. Sohl, and G. Kristensson. Physical limitations on antennas of arbitrary shape. *Proc. R. Soc. A*, **463**, 2589–2607, 2007.

[7] M. Gustafsson, C. Sohl, and G. Kristensson. Illustrations of new physical bounds on linearly polarized antennas. *IEEE Trans. Antennas Propagat.*, **57**(5), 1319–1327, May 2009.

[8] M. Gustafsson and S. Nordebo. Bandwidth, Q factor, and resonance models of antennas. *Progress in Electromagnetics Research*, **62**, 1–20, 2006.

[9] M. Gustafsson, C. Sohl, and S. Nordebo. Physical bounds on the antenna scattering matrix. In *IEEE International Symposium on Antennas and Propagation*. IEEE-AP, San Diego, July 5–12 2008.

[10] G. Hall et al. *The ARRL Antenna Book*. American Radio Relay League, 1984.

[11] J. E. Hansen, editor. *Spherical Near-Field Antenna Measurements*. Number 26 in IEE electromagnetic waves series. Peter Peregrinus Ltd., Stevenage, UK, 1988. ISBN: 0-86341-110-X.

[12] W. Kahn and H. Kurss. Minimum-scattering antennas. *IEEE Trans. Antennas Propagat.*, **13**(5), 671–675, 1965.

[13] R. E. Kleinman and T. B. A. Senior. Rayleigh scattering. In V. V. Varadan and V. K. Varadan, editors, *Low and high frequency asymptotics*, volume 2 of *Handbook on Acoustic, Electromagnetic and Elastic Wave Scattering*, chapter 1, pages 1–70. Elsevier Science Publishers, Amsterdam, 1986.

[14] H. M. Nussenzveig. *Causality and dispersion relations.* Academic Press, London, 1972.

[15] S. Silver. *Microwave Antenna Theory and Design*, volume 12 of *Radiation Laboratory Series.* McGraw-Hill, New York, 1949.

[16] C. Sohl and M. Gustafsson. A priori estimates on the partial realized gain of Ultra-Wideband (UWB) antennas. *Quart. J. Mech. Appl. Math.*, **61**(3), 415–430, 2008.

[17] C. Sohl, M. Gustafsson, and G. Kristensson. Physical limitations on broadband scattering by heterogeneous obstacles. *J. Phys. A: Math. Theor.*, **40**, 11165–11182, 2007.

[18] A. D. Yaghjian and S. R. Best. Impedance, bandwidth, and Q of antennas. *IEEE Trans. Antennas Propagat.*, **53**(4), 1298–1324, 2005.